

An Application of Bayesian Variable Selection to Spatial Concurrent Linear Models

Zuofeng Shang*

Environmental Change Initiative, and

Department of Applied and Computational Mathematics and Statistics

University of Notre Dame, Notre Dame, USA

and

Murray K. Clayton

Department of Statistics

University of Wisconsin-Madison, Madison, USA

Abstract

Spatial concurrent linear models, in which the model coefficients are spatial processes varying at a local level, are flexible and useful tools for analyzing spatial data. One approach places stationary Gaussian process priors on the spatial processes, but in applications the data may display strong nonstationary patterns. In this article, we propose a Bayesian variable selection approach based on wavelet tools to address this problem. The proposed approach does not involve any stationarity assumptions on the priors, and instead we impose a mixture prior directly on each wavelet coefficient. We introduce an option to control the priors such that high resolution coefficients are more likely to be zero. Computationally efficient MCMC procedures are provided to address posterior sampling, and uncertainty in the estimation is assessed through posterior means and standard deviations. Examples based on simulated data demonstrate the estimation accuracy and advantages of the proposed method. We also illustrate the performance of the proposed method for real data obtained through remote sensing.

Keywords and phrases: Bayesian estimation; Satellite images; Haar wavelet; Mixture prior; spike and slab prior; Blockwise Gibbs sampler; Inference.

*Corresponding author: zshang@nd.edu

1 Introduction

One objective in spatial data analysis is to study the relationship between explanatory (input) and response (output) variables through an appropriate model. Our interest arises when the input and output are represented by images consisting of large numbers of pixels, as might be obtained in remote sensing (satellite) imagery. A particular example consists of gypsy moth defoliation data which were obtained by satellite from a region in the Appalachian Mountains in June-July 2006. (See Townsend *et al.* (2004) for more details.) For these data, the response is an image representing gypsy moth defoliation rates of oak trees. It is of interest to relate these rates to elevation, which can also be represented as an image (Figure 1). Several authors have observed that defoliation rate generally increases with elevation (see, e.g., Kleiner and Montgomery, 1994).

Zhang *et al.* (2011) assessed that relationship by using a concurrent linear model with general form

$$y(\mathbf{s}) = A(\mathbf{s}) + x_1(\mathbf{s})B_1(\mathbf{s}) + \dots + x_K(\mathbf{s})B_K(\mathbf{s}) + \epsilon(\mathbf{s}), \quad (1.1)$$

where \mathbf{s} indicates a spatial location, A is the intercept surface, B_1, \dots, B_K are the slope surfaces, and $\epsilon(\mathbf{s})$ indicates the error term. In the defoliation rate data (Figure 1), $K = 1$.

One challenge with these data is the very large number of observations, and the potentially large number of parameters to estimate. Zhang *et al.* (2011) applied a wavelet transformation to both the intercept and slope surfaces and proposed using LASSO to estimate the model parameters. Besides computational facility, Zhang's approach does not require the coefficient surfaces A, B_1, \dots, B_K to be stationary, and hence, can be applied to a broad range of situations such as the defoliation rate data displayed in Figure 1 which appears to involve complex nonstationary patterns. However, it is hard to use Zhang's approach to conduct inference, which is the motivation of the present work. In this paper, we consider two major generalizations. First, we expand on the work of Zhang *et al.* (2011) by using a Bayesian framework based on Bayesian variable selection (BVS) that allows for more direct inferences on the estimates. Second, this naturally results in a generalization of previous work on BVS in the wavelet-based one-dimensional time setting to a two-dimensional spatial setting. The result is an approach that is flexible and efficient for modeling the relationships between image data involving complex patterns. Furthermore, to address the large sample size and complex dependence structure of these spatial data, we implement an efficient Gibbs sampler. Because we reply on Zhang's modeling strategy in this paper, we briefly outline some notions

of wavelets. We also briefly review some previous work on BVS.

Wavelets are sets of functions whose shifts and scales form a set of basis functions. In particular, a bivariate wavelet consists of three functions denoted by φ^r for $r = 1, 2, 3$. When the φ^r s are chosen correctly, any two-dimensional square integrable function f can be represented by the following approximation,

$$f(\mathbf{s}) \approx f_0 + \sum_{r=1}^3 \sum_{j=0}^J \sum_{k \in \Lambda_j} f_{jk}^r \varphi_{jk}^r(\mathbf{s}), \quad \mathbf{s} \in [0, 1) \times [0, 1), \quad (1.2)$$

where J is the maximal level of decomposition, $\varphi_{jk}^r(\mathbf{s}) = 2^j \varphi^r(2^j \mathbf{s} - k)$ is the scale-and-shift transform of function φ^r , and $\Lambda_j = \{(k_1, k_2) | k_1, k_2 = 0, 1, \dots, 2^j - 1\}$ is the index set for k at resolution level j . $\{\varphi_{jk}^r\}$ is called the wavelet basis and $\{f_0, f_{jk}^r\}$ are the wavelet coefficients. The transform from f to $\{f_0, f_{jk}^r\}$ is called the two-dimensional discrete wavelet transform (DWT). If we want to include more details or information from the image f , a large J is preferred, and in fact, when J goes to infinity, the representation (1.2) will be exact (see Daubechies 1992), which means that all of the information on f is included. When f is locally flat, a DWT can result in a very sparse coefficient set in the sense that most of the wavelet coefficients of f are zero.

A special example is the Haar wavelet, which generates orthonormal wavelet basis functions being constant on their supports. Using Haar wavelet, we can express $A(\mathbf{s}) = W(\mathbf{s})\mathbf{a}$ and $B_k(\mathbf{s}) = W(\mathbf{s})\mathbf{b}_k$, where \mathbf{a} and \mathbf{b}_k are d -dimensional vectors of wavelet coefficients, and $W(\mathbf{s})$ is a row vector of length d corresponding to the Haar DWT at location \mathbf{s} . Note that if J -level wavelet expansions are used, then $d = 4^{J+1}$. Therefore, the total number of wavelet coefficients is $m = (K + 1)d = (K + 1)4^{J+1}$. If n pixels of the image are observed, then model (1.1) can be rewritten as

$$\mathbf{y} = X\beta + \epsilon, \quad (1.3)$$

where $\mathbf{y} = (y(\mathbf{s}_1), \dots, y(\mathbf{s}_n))'$, $X = [W, \tilde{\mathbf{x}} \circ W]$ is an $n \times m$ design matrix with “ \circ ” denoting the Schur product, W is an $n \times d$ matrix with rows $W(\mathbf{s}_i)$, $\beta = [\mathbf{a}', \mathbf{b}'_1, \dots, \mathbf{b}'_K]'$ is an m -vector, $\tilde{\mathbf{x}} = [x_k(\mathbf{s}_i)]_{1 \leq k \leq K, 1 \leq i \leq n}$ is an $n \times K$ matrix, and x_k is the k -th component of \mathbf{x} . In order to capture fine details, m might be large.

Next, we briefly review some references on BVS. Unless otherwise stated, we use β_j for $j = 1, \dots, m$ to denote the components of β . One version of BVS was proposed by George and McCulloch (1993), based on the model

$$(a) \quad \mathbf{y} | \beta, \sigma^2 \sim N(X\beta, \sigma^2 I),$$

$$(b) \beta_j | \gamma_j \stackrel{cond. ind.}{\sim} (1 - \gamma_j)N(0, \tau_j^2) + \gamma_j N(0, c_j \tau_j^2),$$

$$(c) \gamma_j \stackrel{ind.}{\sim} \text{Bernoulli}(p_j).$$

where $c_j > 0$, $\tau_j^2 > 0$ and $p_j \in (0, 1)$ are fixed, “*ind.*” means *independence* and “*cond. ind.*” means *conditional independence*. Each γ_j is a 0-1 variable and γ_j and 0 are related with inclusion and exclusion of β_j respectively when τ_j s and c_j s are set at a small and a large value respectively. The authors gave procedures for selecting c_j and τ_j^2 and defined the best model to be $\hat{\gamma} = \arg \max_{\gamma} p(\gamma | \text{data})$. A Gibbs sampler was used for computations.

Different BVS procedures have been proposed based on variations of (a)–(c). For instance, Smith and Kohn (1996) applied BVS to spline regression models. They assumed that a signal vector $\mathbf{f} = (f(s_1), \dots, f(s_n))'$ was observed with noise and considered the model $\mathbf{y} = \mathbf{f} + \epsilon$, where \mathbf{y} is the vector of observations and ϵ is the vector of noise. Using spline basis expansions they rewrote this model as $\mathbf{y} = X\beta + \epsilon$, where β is a vector of spline coefficients and X is a matrix induced by the spline basis functions. They proposed the following variation of (b),

$$(b)' \beta_j | \gamma_j \stackrel{cond. ind.}{\sim} (1 - \gamma_j)\delta_0 + \gamma_j N(0, c_j \sigma^2),$$

where δ_0 is the point mass measure at zero and $c_j > 0$ is fixed. Prior (b)' is known as the spike and slab prior. They also developed a Gibbs sampler for computation based on the model (a), (b)', (c). Subsequently, Clyde *et al.* (1998) and Clyde and George (2000) considered similar models in different settings such as the one-dimensional wavelet regression problem.

Another strategy for coefficient selection was implemented for Gabor regression over the time domain by Wolfe *et al.* (2004). The principal difference in the Gabor approach and the wavelet approach is that the Gabor system forms an over-complete basis whereas the wavelet basis is complete. Wavelet approach is useful since we may choose the wavelet basis to be orthogonal which may result in computational convenience. The authors used Ising and Markov chain priors to model the dependence structure among the Gabor coefficients. In order to accommodate more flexibility, they proposed the following variations of (b)' and (c),

$$(b)'' \beta_j | \gamma_j, \tau_j^2 \stackrel{cond. ind.}{\sim} (1 - \gamma_j)\delta_0 + \gamma_j N(0, \tau_j^2), \quad \tau_j^2 \stackrel{ind.}{\sim} \text{Inverse Gamma}$$

$$(c)' \gamma \sim p(\gamma),$$

where β_j s denote the Gabor coefficients, τ_j^2 may vary with β_j , and $p(\gamma)$ varies among the

Bernoulli, Ising and Markov chain priors. Then, based on model (a), (b)'', (c)', the authors applied a Gibbs sampler to approximate the β_j s and τ_j^2 s.

Other relevant references include Brown *et al.* (2001) who used BVS based on a one-dimensional wavelet approach to analyze curve data over time, and proposed a Metropolis-Hasting type sampler for posterior computation. Brown *et al.* (2002) generalized the model proposed by George and McCulloch (1993) to a multi-dimensional situation, and proposed an estimation procedure based on prediction. Nott and Green (2004) discussed several computational issues related to BVS. Yuan and Lin (2005) explored the relationship between LASSO and Bayesian approaches through a variable selection view. Smith and Fahrmeir (2007) proposed a piecewise local linear model to analyze fMRI data, and performed BVS by using Ising priors on each local linear model. Wheeler (2009) proposed geographically weighted LASSO to analyze spatial data. Wheeler and Waller (2009) proposed a Bayesian framework (built upon a parametric model) analogous to ridge regression to analyze spatial concurrent linear model, while the proposed approach here relies on a nonparametric wavelet approach which can capture the local behaviors of the estimates. There are also several theoretical results on BVS including asymptotics of the posterior density: Jiang (2007); Jiang and Tanner (2008), in which the authors proved density consistency under some functional metric; and posterior model consistency: Fernández *et al.* (2001); Casella *et al.* (2009); Liang *et al.* (2008); Moreno *et al.* (2010); and Shang and Clayton (2011), in which the authors proved that, under suitable conditions, the posterior probability of the true model converges to one as the sample size grows to infinity.

The remainder of this paper is structured as follows. In Section 2, two different Bayesian models will be established and the corresponding MCMC algorithms for posterior sampling will be described. In Section 3, simulation and real data examples demonstrating the applications of our models and algorithms will be provided. In particular, we discuss the matter of making inferences for the slope and intercept surfaces. Section 4 contains discussion, and the supplement material contains technical details.

2 Models and Algorithms

In this section, we develop our specific modeling approach. To simplify the details, we only consider $K = 1$ in model (1.1), i.e., only one slope surface is involved, although generalization

to multiple slope surfaces is not difficult. Thus, model (1.1) becomes the following model with a single covariate surface x

$$y(\mathbf{s}_i) = A(\mathbf{s}_i) + x(\mathbf{s}_i)B(\mathbf{s}_i) + \epsilon(\mathbf{s}_i), \quad i = 1, \dots, n, \quad (2.1)$$

where $n = 4^{J+2}$, $\{\mathbf{s}_i\}_{i=1}^n = \{(2^{-J-2}k_1, 2^{-J-2}k_2) | k_1, k_2 = 0, 1, \dots, 2^{J+2} - 1\}$ is the set of locations evenly spaced over $[0, 1) \times [0, 1)$, and the $\epsilon(\mathbf{s}_i)$ s $\stackrel{iid.}{\sim} N(0, \sigma^2)$. By performing a two-dimensional Haar DWT with maximal level of decomposition J on A and B , model (2.1) can be written as a linear model $\mathbf{y} = X\beta + \epsilon$, which is a special case of (1.3) when $K = 1$. Here, X is the $n \times m$ design matrix induced by Haar DWT with $m = 2(4^{J+1})$, $\epsilon \sim N(\mathbf{0}, \sigma^2 I_n)$ is an n -vector of errors, and $\beta = [\mathbf{a}', \mathbf{b}']'$ with \mathbf{a} and \mathbf{b} being the $(m/2)$ -vectors of wavelet coefficients corresponding to surfaces A and B .

Instead of imposing stationary prior distributions in the spatial domain of A and B , we assign mixture priors in the wavelet domain β corresponding to the resolution levels, which may produce nonstationary priors for A and B and accommodate more complex structures in spatial domain. Even if the components of β are assumed to be *a priori* independent, when $\mathbf{s} \neq \tilde{\mathbf{s}}$, $A(\mathbf{s})$ and $A(\tilde{\mathbf{s}})$, $B(\mathbf{s})$ and $B(\tilde{\mathbf{s}})$ may still be spatially correlated. In fact, as \mathbf{s} and $\tilde{\mathbf{s}}$ become closer in space, $A(\mathbf{s})$ and $A(\tilde{\mathbf{s}})$, $B(\mathbf{s})$ and $B(\tilde{\mathbf{s}})$ will share more common wavelet coefficients in their wavelet expansions, which makes their spatial correlations stronger.

We will consider two different Bayesian models and provide corresponding MCMC algorithms. In both models, we assume

$$\mathbf{y}|X, \beta, \sigma^2 \sim N(X\beta, \sigma^2 I_n), \quad 1/\sigma^2 \sim \chi_\nu^2,$$

where ν is a fixed hyperparameter. Let $\gamma = (\gamma_1, \dots, \gamma_m)$ with γ_j s being the 0-1 Bernoulli variables indicating the exclusion and inclusion of β_j s. In both models we place Bernoulli priors on γ , i.e., $p(\gamma_1, \dots, \gamma_m) = \prod_{j=1}^m \theta_j^{\gamma_j} (1 - \theta_j)^{1-\gamma_j}$, where $\theta_j = p(\gamma_j = 1)$ is the inclusion probability. However, we consider different priors for β .

Our first Bayesian model requires all the nonzero components of β to possess a common prior variance τ^2 . Given γ and τ^2 , the β_j s are independent with mixture priors.

$$\text{Model I:} \quad \beta_j | \gamma_j, \tau^2 \sim (1 - \gamma_j)\delta_0 + \gamma_j N(0, \tau^2), \quad 1/\tau^2 \sim \chi_\mu^2,$$

where μ is fixed. Based on Model I, the posterior distribution of $(\beta, \gamma, \sigma^2, \tau^2)$ is

$$\begin{aligned} & p(\beta, \gamma, \sigma^2, \tau^2 | \mathbf{y}, X) \\ & \propto \left(\frac{1}{\sqrt{2\pi}\sigma} \right)^n \exp(-\|\mathbf{y} - X\beta\|^2 / (2\sigma^2)) \cdot \prod_{j=1}^m \left[\frac{1}{\tau} \phi \left(\frac{\beta_j}{\tau} \right) \right]^{\gamma_j} \delta_0(\beta_j)^{1-\gamma_j} \\ & \cdot \frac{2^{-\nu/2}}{\Gamma(\nu/2)} \sigma^{-\nu-2} \exp(-1/(2\sigma^2)) \cdot \frac{2^{-\mu/2}}{\Gamma(\mu/2)} \tau^{-\mu-2} \exp(-1/(2\tau^2)) p(\gamma), \end{aligned} \quad (2.2)$$

where ϕ is the $N(0, 1)$ probability density function. If $\tau = \sigma$, then Model I is similar to one proposed by Clyde *et al.* (1998) and Li and Zhang (2010). Here we do not assume that the variances of the coefficients are related to σ , which makes our model flexible. A blockwise Gibbs sampler introduced by Godsill and Rayner (1998) and Wolfe *et al.* (2004) will be used to draw samples from the posterior distribution, as we now describe.

Algorithm I. Given a current state $(\beta^{(t)}, \gamma^{(t)}, \sigma^{(t)}, \tau^{(t)})$.

(A) Update (γ, β) :

$$\begin{aligned} p(\gamma_j^{(t+1)} = 1 | \beta_{-j}, \gamma_{-j}, \sigma^{(t)}, \tau^{(t)}, \mathbf{y}, X) &= \frac{1}{1 + \rho_j}, \\ p(\beta_j^{(t+1)} = 0 | \gamma_j^{(t+1)} = 0, \beta_{-j}, \gamma_{-j}, \sigma^{(t)}, \tau^{(t)}, \mathbf{y}, X) &= 1, \\ \beta_j^{(t+1)} | \gamma_j^{(t+1)} = 1, \beta_{-j}, \gamma_{-j}, \sigma^{(t)}, \tau^{(t)}, \mathbf{y}, X &\sim N \left(\frac{u_j}{v_j^2}, \frac{(\sigma^{(t)})^2}{v_j^2} \right), \end{aligned}$$

where $\gamma_{-j} = (\gamma_1^{(t+1)}, \dots, \gamma_{j-1}^{(t+1)}, \gamma_{j+1}^{(t)}, \dots, \gamma_m^{(t)})'$, $\beta_{-j} = (\beta_1^{(t+1)}, \dots, \beta_{j-1}^{(t+1)}, \beta_{j+1}^{(t)}, \dots, \beta_m^{(t)})'$,

$$u_j = (\mathbf{y} - X_{-j}\beta_{-j})' X_j, \quad v_j = \left(X_j' X_j + \frac{(\sigma^{(t)})^2}{(\tau^{(t)})^2} \right)^{1/2}$$

with X_j being the j -th column of X and $X_{-j} = (X_1, \dots, X_{j-1}, X_{j+1}, \dots, X_m)$, and

$$\rho_j = \frac{p(\gamma_j = 0 | \gamma_{-j})}{p(\gamma_j = 1 | \gamma_{-j})} \frac{\tau^{(t)} v_j}{\sigma^{(t)}} \exp \left(-\frac{u_j^2}{2(\sigma^{(t)})^2 v_j^2} \right).$$

(B) Update (σ, τ) :

$$\begin{aligned} (\sigma^{(t+1)})^2 | \gamma^{(t+1)}, \beta^{(t+1)}, \tau^{(t)}, \mathbf{y}, X &\sim IG \left(\frac{n + \nu}{2}, \frac{1 + \|\mathbf{y} - X_{\gamma^{(t+1)}} \beta_{\gamma^{(t+1)}}^{(t+1)}\|_2^2}{2} \right), \\ (\tau^{(t+1)})^2 | \gamma^{(t+1)}, \beta^{(t+1)}, \sigma^{(t+1)}, \mathbf{y}, X &\sim IG \left(\frac{|\gamma^{(t+1)}| + \mu}{2}, \frac{1 + \|\beta^{(t+1)}\|_2^2}{2} \right), \end{aligned}$$

where $IG(a, b)$ denotes the inverse gamma distribution with density $g(x) \propto x^{-a-1} \exp(-b/x)$ for $x > 0$.

The derivation of Algorithm I can be found in the supplement material. Unlike the usual non-blockwise Gibbs sampler, Algorithm I involves no matrix inversion, and hence, is computationally efficient when m is moderate. However, when m is large, a direct application of Algorithm I will still be time-consuming because evaluating the quantity u_j in step (A) involves intensive matrix multiplication. To address this problem, we notice that $V_j = \mathbf{y} - X_{-j}\beta_{-j}$ and $V_{j-1} = \mathbf{y} - X_{-(j-1)}\beta_{-(j-1)}$ satisfy

$$V_j = V_{j-1} + \beta_j^{(t)} X_j - \beta_{j-1}^{(t+1)} X_{j-1}. \quad (2.3)$$

By (2.3), V_j can be obtained directly through V_{j-1} , which is available from the last updating. This effectively avoids unnecessary matrix multiplications in each iteration. A technique similar in spirit to (2.3) to reduce the computational burden was employed by Li and Zhang (2010), who proposed a non-blockwise Gibbs sampler for high-dimensional structured models.

In Model I, the prior variances of the nonzero β_j s have been set to be a common hyperparameter τ^2 , which seems restrictive. Our second Bayesian model overcomes this restriction by introducing different prior variances τ_j^2 s for β_j s. Given γ and τ_j^2 s, we assume the β_j s are independent with mixture priors as follows:

$$\textbf{Model II: } \quad \beta_j | \gamma_j, \tau_j^2 \sim (1 - \gamma_j)\delta_0 + \gamma_j N(0, \tau_j^2), \quad 1/\tau_1^2, \dots, 1/\tau_m^2 \stackrel{iid.}{\sim} \chi_\mu^2,$$

where μ is fixed. Based on Model II, the posterior distribution of $(\beta, \gamma, \sigma^2, \tau_1^2, \dots, \tau_m^2)$ is

$$\begin{aligned} & p(\beta, \gamma, \sigma^2, \tau_1^2, \dots, \tau_m^2 | \mathbf{y}, X) \\ & \propto \left(\frac{1}{\sqrt{2\pi}\sigma} \right)^n \exp(-\|\mathbf{y} - X\beta\|^2 / (2\sigma^2)) \cdot \prod_{j=1}^m \left[\frac{1}{\tau_j} \phi\left(\frac{\beta_j}{\tau_j}\right) \right]^{\gamma_j} \delta_0(\beta_j)^{1-\gamma_j} \\ & \quad \cdot \frac{2^{-\nu/2}}{\Gamma(\nu/2)} \sigma^{-\nu-2} \exp(-1/(2\sigma^2)) \cdot \prod_{j=1}^m \frac{2^{-\mu/2}}{\Gamma(\mu/2)} \tau_j^{-\mu-2} \exp(-1/(2\tau_j^2)) p(\gamma), \end{aligned} \quad (2.4)$$

where ϕ is the $N(0, 1)$ probability density function. Using the blockwise technique, one can draw posterior samples from $p(\beta, \gamma, \sigma^2, \tau_1^2, \dots, \tau_m^2 | \mathbf{y}, X)$ with the following algorithm:

Algorithm II.

Given a current state $(\beta^{(t)}, \gamma^{(t)}, \sigma^{(t)}, \tau_1^{(t)}, \dots, \tau_m^{(t)})$.

(A) Update (γ, β) :

$$p(\gamma_j^{(t+1)} = 1 | \beta_{-j}, \gamma_{-j}, \tau_1^{(t)}, \dots, \tau_m^{(t)}, \sigma^{(t)}, \mathbf{y}, X) = \frac{1}{1 + \rho_j},$$

$$p(\beta_j^{(t+1)} = 0 | \gamma_j^{(t+1)} = 0, \beta_{-j}, \gamma_{-j}, \tau_1^{(t)}, \dots, \tau_m^{(t)}, \sigma^{(t)}, \mathbf{y}, X) = 1,$$

$$\beta_j^{(t+1)} | \gamma_j^{(t+1)} = 1, \beta_{-j}, \gamma_{-j}, \tau_1^{(t)}, \dots, \tau_m^{(t)}, \sigma^{(t)}, \mathbf{y}, X \sim N\left(\frac{u_j}{v_j^2}, \frac{(\sigma^{(t)})^2}{v_j^2}\right),$$

where $\gamma_{-j} = (\gamma_1^{(t+1)}, \dots, \gamma_{j-1}^{(t+1)}, \gamma_{j+1}^{(t)}, \dots, \gamma_m^{(t)})'$, $\beta_{-j} = (\beta_1^{(t+1)}, \dots, \beta_{j-1}^{(t+1)}, \beta_{j+1}^{(t)}, \dots, \beta_m^{(t)})'$,

$$u_j = (\mathbf{y} - X_{-j}\beta_{-j})'X_j, \quad v_j = \left(X_j'X_j + \frac{(\sigma^{(t)})^2}{(\tau_j^{(t)})^2}\right)^{1/2}$$

with X_j being the j -th column of X and $X_{-j} = (X_1, \dots, X_{j-1}, X_{j+1}, \dots, X_m)$, and

$$\rho_j = \frac{p(\gamma_j = 0 | \gamma_{-j}) \tau_j^{(t)} v_j}{p(\gamma_j = 1 | \gamma_{-j}) \sigma^{(t)}} \exp\left(-\frac{u_j^2}{2(\sigma^{(t)})^2 v_j^2}\right).$$

(B) Update τ_j :

$$\begin{aligned} (\tau_j^{(t+1)})^2 | \beta_j^{(t+1)}, \gamma_j^{(t+1)} = 0, \mathbf{y}, X &\sim 1/\chi_\mu^2, \\ (\tau_j^{(t+1)})^2 | \beta_j^{(t+1)}, \gamma_j^{(t+1)} = 1, \mathbf{y}, X &\sim IG\left(\frac{1+\mu}{2}, \frac{1+(\beta_j^{(t+1)})^2}{2}\right), j = 1, \dots, m. \end{aligned}$$

(C) Update σ :

$$(\sigma^{(t+1)})^2 | \gamma^{(t+1)}, \beta^{(t+1)}, \mathbf{y}, X \sim IG\left(\frac{n+\nu}{2}, \frac{1 + \|\mathbf{y} - X_{\gamma^{(t+1)}}\beta_{\gamma^{(t+1)}}\|_2^2}{2}\right).$$

The derivation of Algorithm II is similar to that of Algorithm I. Since $2m + 2$ parameters have been involved in Model I, while $3m + 1$ parameters have been involved in Model II, it takes more time to use Algorithm II than Algorithm I for MCMC sampling. However, Bayesian estimates resulting from Model II may sometimes have better performance than those resulting from Model I, which will be seen in next section. To reduce computational cost, a technique similar to (2.3) will also be applied to Algorithm II.

3 Numerical Results

In this section, we apply the Bayesian methods developed in Section 2 to the concurrent linear model (2.1) and illustrate these methods with simulated and real datasets. In Section 3.1, we consider the problem of reconstructing both intercept and slope surfaces, and use them to obtain the fitted response surface. We assess the performance of Models I and

II through four criteria: squared bias, variance, mean square error for the estimate of the coefficient surface, and mean square error for the response. Comparison with the LASSO approach proposed by Zhang *et al.* (2011) will also be demonstrated. In Section 3.2, we try to find the locations where the relationship between the response and the covariate is strong. In Section 3.3, we apply our methods to gypsy moth defoliation data.

Let $\{\mathbf{s}_i\}_{i=1}^n$ be the lattice set of locations specified in Section 2. Denote $\mathbf{A} = (A(\mathbf{s}_1), \dots, A(\mathbf{s}_n))'$ and $\mathbf{B} = (B(\mathbf{s}_1), \dots, B(\mathbf{s}_n))'$. After obtaining the estimates $\hat{\mathbf{a}}$ and $\hat{\mathbf{b}}$ of \mathbf{a} and \mathbf{b} , we perform an inverse DWT to obtain the estimates of \mathbf{A} and \mathbf{B} through $\hat{\mathbf{A}} = W\hat{\mathbf{a}}$ and $\hat{\mathbf{B}} = W\hat{\mathbf{b}}$, where $W \in \mathbb{R}^{n \times \frac{m}{2}}$ corresponds to the two-dimensional Haar DWT and satisfies $W'W = I_{m/2}$.

The Markov chains simulated from posterior likelihoods (2.2) and (2.4) will converge quickly if the initial points of these chains are carefully selected. Here, we adopt an empirical procedure for this purpose. We first let $\hat{\beta} = (X'X)^{-1}X'\mathbf{y}$ be the least squares estimate, then we choose the initial point $\beta^{(0)}$ for the Markov chains as a draw from $N(\hat{\beta}, \tilde{\sigma}^2 I_m)$ with $\tilde{\sigma}^2$ predetermined to be the variance of $\beta^{(0)}$.

3.1 Assessing the Performance of Models I and II

We assessed the performance of Models I and II through the numerical results by Algorithms I and II. We chose the true intercept surface to be

$$A(s_1, s_2) = \begin{cases} 1, & 0 \leq s_1 < 0.5, 0 \leq s_2 < 0.5 \\ 4, & 0.5 \leq s_1 < 1, 0 \leq s_2 < 0.5 \\ 7, & 0 \leq s_1 < 0.5, 0.5 \leq s_2 < 1 \\ 10, & 0.5 \leq s_1 < 1, 0.5 \leq s_2 < 1, \end{cases}$$

and considered two different slope surfaces: (Case I)

$$B(s_1, s_2) = \begin{cases} 1, & 0 \leq s_1 < 0.47, 0 \leq s_2 < 0.5 \\ 3, & 0.47 \leq s_1 < 1, 0 \leq s_2 < 0.5 \\ 5, & 0 \leq s_1 < 0.5, 0.5 \leq s_2 < 1 \\ 7, & 0.5 \leq s_1 < 1, 0.5 \leq s_2 < 1, \end{cases}$$

and (Case II) $B(s_1, s_2) = 4 \sin(2\pi s_1) \cos(2\pi s_2)$, for $0 \leq s_1, s_2 < 1$.

To further explore the role played by the covariate surface, three covariate surfaces with different types of oscillation were considered:

$$x_a(s_1, s_2) = 4 \sin(4\pi(s_1 + s_2)), \quad (3.1)$$

$$x_b(s_1, s_2) = 4 \sin(10\pi(s_1 + s_2)), \quad (3.2)$$

$$x_c(s_1, s_2) = 4 \sin(15\pi(s_1 + s_2)), \quad 0 \leq s_1, s_2 \leq 1. \quad (3.3)$$

We chose $J = 3$ and generated data from model (2.1) with $\sigma = 1$. Therefore, $n = 1024$ and $m = 512$. There are 3 nonzero wavelet coefficients for A . In Case I, B is locally flat corresponding to 3 nonzero wavelet coefficients. (Recall that we are using Haar wavelets.) However, in Case II, B has little local flatness and all 256 wavelet coefficients of B are nonzero. We fixed $\mu = \nu = 6$. Let $\{a_0, a_{jk}^r | r = 1, 2, 3, j = 0, 1, \dots, J, k \in \Lambda_j\}$ and $\{b_0, b_{jk}^r | r = 1, 2, 3, j = 0, 1, \dots, J, k \in \Lambda_j\}$ be the components of \mathbf{a} and \mathbf{b} , and $\gamma_0^a = I(a_0 \neq 0)$, $\gamma_0^b = I(b_0 \neq 0)$, $\gamma_{jkr}^a = I(a_{jk}^r \neq 0)$, $\gamma_{jkr}^b = I(b_{jk}^r \neq 0)$, where j denotes the resolution level of the wavelet coefficients and Λ_j denotes the collection of the indexes of the wavelet coefficients at the j -th resolution level. We considered the following three different Bernoulli priors for γ .

Prior (1):

$$p(\gamma_0^a = 1) = p(\gamma_0^b = 1) = 0.5, \quad p(\gamma_{jkr}^a = 1) = p(\gamma_{jkr}^b = 1) = 0.5\phi^j, \quad r = 1, 2, 3, j = 0, \dots, J, \quad k \in \Lambda_j.$$

Prior (2):

$$p(\gamma_0^a = 1) = p(\gamma_0^b = 1) = 0.5, \quad p(\gamma_{jkr}^a = 1) = 0.5\phi^j, \quad p(\gamma_{jkr}^b = 1) = 0.5, \quad r = 1, 2, 3, j = 0, \dots, J, \quad k \in \Lambda_j.$$

Prior (3):

$$p(\gamma_0^a = 1) = p(\gamma_0^b = 1) = 0.5, \quad p(\gamma_{jkr}^a = 1) = 0.5\phi^{8j}, \quad p(\gamma_{jkr}^b = 1) = 0.5, \quad r = 1, 2, 3, j = 0, \dots, J, \quad k \in \Lambda_j.$$

Different ϕ values and the resultant Bernoulli priors can produce difference levels of sparsity in the estimates. Thus, the selection of ϕ is purely empirical depending on how much sparsity is expected in the estimates. For instance, if a practitioner expects that the estimate should be fairly sparse, then one can choose to be relatively smaller such as $\phi = 0.7$; otherwise, one may just use $\phi = 0.9$ to produce certain amount of sparsity or even use $\phi = 1$ to fully let the model drive the amount of sparsity in the estimates since $\phi = 1$ corresponds to indifference Bernoulli prior for the coefficients

We considered $\phi = 1, 0.9, 0.8, 0.7$. Note that when $\phi = 1$, Priors (1)–(3) all become indifference priors. We applied Prior (1) to Case I, and applied Priors (2) and (3) to Case II. Prior (1) puts smaller weights on the higher level wavelet coefficients of both surfaces A and B so that they have larger prior probability to be zero, while Priors (2) and (3) only do this for surface A but assign neutral probabilities to the wavelet coefficients of surface B .

For each of the covariate surfaces (3.1)–(3.3) and for both Cases I and II, we repeated the simulations $L = 50$ times. For the l -th replication with $l = 1, \dots, L$, Markov chains with length 5000 were generated from the posterior distribution (2.2), and the first 2500 served as burn-ins. Gelman-Rubin’s factors (see Gelman *et al.*, 2003) for all chains were below 1.1, suggesting that all chains converged well. The estimates \hat{A}^l and \hat{B}^l of A and B based on the l -th replication were obtained through averaging the last 2500 posterior samples.

To assess performance, we borrowed an idea from Fan *et al.* (2010) to calculate the squared bias, variance and mean square errors of the estimates. To state our method, we let \hat{A}_i^l , \hat{B}_i^l , A_i and B_i be the values of \hat{A}^l , \hat{B}^l , A and B at pixel $\tilde{\mathbf{s}}_i$ with $\{\tilde{\mathbf{s}}_i\} = \{(s_1/100, s_2/100) | s_1, s_2 = 0, 1, \dots, 99\}$ being the 100×100 uniform grid of pixels over $[0, 1) \times [0, 1)$. Thus, there are $N = 10^4$ pixels being evaluated. Note that $\{\tilde{\mathbf{s}}_i\}$ have been chosen to be different from the locations where data were drawn for the purposes of assessing the performance of the estimates at new locations. We define the average squared bias to be

$$Bias_A^2 = \frac{1}{N} \sum_{i=1}^N \left(\sum_{l=1}^L \frac{\hat{A}_i^l - A_i}{L} \right)^2,$$

$$Bias_B^2 = \frac{1}{N} \sum_{i=1}^N \left(\sum_{l=1}^L \frac{\hat{B}_i^l - B_i}{L} \right)^2,$$

and define the average variance to be

$$Var_A = \frac{1}{N} \sum_{i=1}^N \sum_{l=1}^L \left(\hat{A}_i^l - \frac{1}{L} \sum_{l=1}^L \hat{A}_i^l \right)^2 / L,$$

$$Var_B = \frac{1}{N} \sum_{i=1}^N \sum_{l=1}^L \left(\hat{B}_i^l - \frac{1}{L} \sum_{l=1}^L \hat{B}_i^l \right)^2 / L.$$

The average mean square errors for A , B are then defined to be $MSE_A = Bias_A^2 + Var_A$ and $MSE_B = Bias_B^2 + Var_B$. The average mean square error for the response is defined to be $MSE_y = \sum_{i=1}^N \sum_{l=1}^L \left(\hat{A}_i^l + x_i \hat{B}_i^l - (A_i + x_i B_i) \right)^2 / (NL)$, where $x_i = x(\tilde{\mathbf{s}}_i)$.

We first assessed the performance of Model I with Algorithm I. Tables 1 and 2 summarize the average squared bias, variance and mean square error of the estimates by using both Algorithm I and LASSO. Since Priors (2) and (3) coincide with each other when $\phi = 1$, we only recorded the results corresponding to Prior (2) when $\phi = 1$. Several findings result from these tables. First, for Case I where both A and B are piecewise constant, the Bayesian estimates corresponding to all the covariate surfaces x_a , x_b and x_c have similar performance

in terms of MSE_A , MSE_B and MSE_y . For estimating A , the Bayesian method results in smaller mean square errors than LASSO, while for estimating B , the Bayesian and LASSO methods result in comparable mean square errors. Second, for Case II where A is piecewise constant but B is smooth, the Bayesian estimates corresponding to x_c are slightly better than those corresponding to x_a and x_b in terms of MSE_A and MSE_B . Zhang *et al.* (2011) observed similar effects of the covariate surfaces on the LASSO estimates. We can also see that, for $\phi = 0.9, 0.8, 0.7$, Prior (3) results in smaller MSE_A than Prior (2). Compared with LASSO, the Bayesian approach corresponding to Prior (3) produces smaller MSE_A , but produces slightly larger MSE_B . Third, for both Priors (2) and (3), when ϕ decreases, the average variances of the posterior estimates of both A and B decrease.

Surface	Method	$Bias_A^2$	$Bias_B^2$	Var_A	Var_B	MSE_A	MSE_B	MSE_y
x_a	$\phi = 1$	0.0004	0.0600	0.0146	0.0010	0.0149	0.0610	0.0223
	$= 0.9$	0.0002	0.0600	0.0091	0.0007	0.0093	0.0607	0.0150
	$= 0.8$	0.0002	0.0601	0.0072	0.0006	0.0074	0.0606	0.0115
	$= 0.7$	0.0002	0.0601	0.0054	0.0005	0.0056	0.0605	0.0094
	LASSO	0.0389	0.0599	0.0038	0.0088	0.0427	0.0687	0.0864
x_b	$\phi = 1$	0.0002	0.0601	0.0132	0.0008	0.0134	0.0609	0.0209
	$= 0.9$	0.0001	0.0601	0.0086	0.0006	0.0087	0.0607	0.0140
	$= 0.8$	0.0001	0.0601	0.0064	0.0005	0.0065	0.0606	0.0108
	$= 0.7$	0.0001	0.0601	0.0051	0.0004	0.0052	0.0605	0.0089
	LASSO	0.0312	0.0595	0.0034	0.0061	0.0346	0.0656	0.0754
x_c	$\phi = 1$	0.0002	0.0603	0.0131	0.0010	0.0133	0.0613	0.0216
	$= 0.9$	0.0001	0.0602	0.0082	0.0007	0.0083	0.0610	0.0145
	$= 0.8$	0.0001	0.0602	0.0060	0.0006	0.0061	0.0608	0.0111
	$= 0.7$	0.0001	0.0602	0.0046	0.0005	0.0047	0.0607	0.0090
	LASSO	0.0341	0.0602	0.0038	0.0044	0.0379	0.0646	0.0731

Table 1: Average squared bias, variance and mean square error related to Case I when Bayesian and LASSO approaches have been applied. For the Bayesian approach, Model I with Algorithm I has been implemented and Prior (1) has been imposed on the vector of Bernoulli variables γ .

To examine Model II with Algorithm II, we repeated the simulations 50 times and each time generated 5000 MCMC samples based on the posterior distribution (2.4). We then treated the first half as burn-ins. Convergence was monitored through Gelman-Rubin's factors. Tables 3 and 4 summarize the results of using Algorithm II. Comparing Tables 1 and 3, and Tables 2 and 4, two observations can be made: (1) for Case I in which B is piecewise constant, Model I and Model II result in comparable MSE_A and MSE_B , while Model I corresponds to slightly smaller MSE_y ; (2) for Case II in which B is smooth, Model II outperforms Model I in terms of MSE_A , MSE_B and MSE_y .

Surface	Method		$Bias_A^2$	$Bias_B^2$	Var_A	Var_B	MSE_A	MSE_B	MSE_y	
x_a	Prior (2)	$\phi = 1$	0.8216	0.3064	0.6070	0.0768	1.4286	0.3832	0.9386	
		$= 0.9$	0.3351	0.2641	0.3963	0.0591	0.7314	0.3232	0.9582	
		$= 0.8$	0.1473	0.2479	0.1629	0.0400	0.3103	0.2879	0.9732	
		$= 0.7$	0.0828	0.2429	0.1196	0.0370	0.2023	0.2799	0.9872	
	Prior (3)	$\phi = 0.9$	0.0237	0.2403	0.0336	0.0298	0.0573	0.2702	1.0124	
		$= 0.8$	0.0144	0.2405	0.0139	0.0285	0.0283	0.2691	1.0281	
		$= 0.7$	0.0137	0.2411	0.0121	0.0284	0.0259	0.2695	1.0305	
	LASSO		0.1298	0.1987	0.0222	0.0355	0.1520	0.2342	0.8599	
	x_b	Prior (2)	$\phi = 1$	0.0952	0.2069	0.1149	0.0318	0.2101	0.2387	0.9641
			$= 0.9$	0.0691	0.2037	0.0817	0.0304	0.1507	0.2341	0.9696
$= 0.8$			0.0535	0.2034	0.0596	0.0294	0.1131	0.2327	0.9789	
$= 0.7$			0.0440	0.2033	0.0440	0.0286	0.0880	0.2319	0.9879	
Prior (3)		$\phi = 0.9$	0.0313	0.2060	0.0166	0.0269	0.0479	0.2329	1.0134	
		$= 0.8$	0.0288	0.2065	0.0076	0.0267	0.0364	0.2332	1.0270	
		$= 0.7$	0.0285	0.2068	0.0061	0.0268	0.0346	0.2336	1.0302	
LASSO		0.1212	0.1885	0.0067	0.0237	0.1279	0.2122	0.9374		
x_c		Prior (2)	$\phi = 1$	0.0427	0.1994	0.0707	0.0286	0.1134	0.2280	1.0131
			$= 0.9$	0.0248	0.1986	0.0486	0.0271	0.0734	0.2257	1.0271
	$= 0.8$		0.0149	0.1990	0.0345	0.0265	0.0494	0.2255	1.0428	
	$= 0.7$		0.0090	0.1993	0.0243	0.0261	0.0333	0.2253	1.0569	
	Prior (3)	$\phi = 0.9$	0.0025	0.1997	0.0088	0.0263	0.0113	0.2260	1.0893	
		$= 0.8$	0.0015	0.1999	0.0032	0.0260	0.0047	0.2259	1.1052	
		$= 0.7$	0.0014	0.1999	0.0029	0.0261	0.0043	0.2259	1.1075	
	LASSO		0.0549	0.1941	0.0039	0.0199	0.0588	0.2139	1.2012	

Table 2: Average squared bias, variance and mean square error related to Case II when Bayesian and LASSO approaches have been applied. For the Bayesian approach, Model I with Algorithm I has been implemented and Priors (2) and (3) have been imposed on the vector of Bernoulli variables γ .

Surface	Method	$Bias_A^2$	$Bias_B^2$	Var_A	Var_B	MSE_A	MSE_B	MSE_y
x_a	$\phi = 1$	0.0003	0.0604	0.0132	0.0067	0.0135	0.0670	0.0863
	$= 0.9$	0.0002	0.0602	0.0103	0.0046	0.0105	0.0648	0.0639
	$= 0.8$	0.0002	0.0601	0.0079	0.0033	0.0080	0.0633	0.0466
	$= 0.7$	0.0001	0.0600	0.0061	0.0023	0.0062	0.0623	0.0333
x_b	$\phi = 1$	0.0006	0.0601	0.0188	0.0075	0.0194	0.0676	0.0909
	$= 0.9$	0.0004	0.0601	0.0137	0.0054	0.0141	0.0655	0.0669
	$= 0.8$	0.0003	0.0601	0.0100	0.0039	0.0103	0.0640	0.0486
	$= 0.7$	0.0002	0.0601	0.0073	0.0028	0.0075	0.0628	0.0346
x_c	$\phi = 1$	0.0004	0.0598	0.0217	0.0082	0.0221	0.0680	0.0933
	$= 0.9$	0.0003	0.0598	0.0152	0.0059	0.0155	0.0657	0.0680
	$= 0.8$	0.0002	0.0598	0.0106	0.0042	0.0108	0.0640	0.0488
	$= 0.7$	0.0001	0.0598	0.0075	0.0030	0.0076	0.0628	0.0345

Table 3: Average squared bias, variance and mean square error related to Case I when a Bayesian approach has been applied. Model II with Algorithm II has been implemented and Prior (1) has been imposed on the vector of Bernoulli variables γ .

Surface	Method	$Bias_A^2$	$Bias_B^2$	Var_A	Var_B	MSE_A	MSE_B	MSE_y	
x_a	Prior (2)	$\phi = 1$	0.0510	0.2212	0.0222	0.0232	0.0733	0.2444	0.9304
		$= 0.9$	0.0451	0.2187	0.0206	0.0234	0.0657	0.2421	0.9356
		$= 0.8$	0.0382	0.2168	0.0187	0.0236	0.0569	0.2404	0.9398
		$= 0.7$	0.0342	0.2151	0.0181	0.0238	0.0523	0.2389	0.9436
	Prior (3)	$\phi = 0.9$	0.0221	0.2109	0.0168	0.0251	0.0389	0.2360	0.9500
		$= 0.8$	0.0199	0.2102	0.0161	0.0253	0.0360	0.2355	0.9526
		$= 0.7$	0.0203	0.2103	0.0163	0.0253	0.0366	0.2356	0.9531
x_b	Prior (2)	$\phi = 1$	0.0200	0.1846	0.0112	0.0218	0.0312	0.2064	0.9020
		$= 0.9$	0.0162	0.1852	0.0088	0.0213	0.0250	0.2065	0.9035
		$= 0.8$	0.0143	0.1848	0.0072	0.0214	0.0215	0.2062	0.9080
		$= 0.7$	0.0134	0.1845	0.0060	0.0215	0.0194	0.2060	0.9115
	Prior (3)	$\phi = 0.9$	0.0133	0.1828	0.0048	0.0222	0.0181	0.2050	0.9232
		$= 0.8$	0.0134	0.1828	0.0046	0.0223	0.0180	0.2051	0.9270
		$= 0.7$	0.0133	0.1829	0.0046	0.0223	0.0179	0.2052	0.9280
x_c	Prior (2)	$\phi = 1$	0.0093	0.1811	0.0114	0.0203	0.0207	0.2014	0.9373
		$= 0.9$	0.0052	0.1808	0.0085	0.0204	0.0138	0.2013	0.9551
		$= 0.8$	0.0029	0.1808	0.0065	0.0204	0.0095	0.2012	0.9663
		$= 0.7$	0.0015	0.1807	0.0052	0.0203	0.0067	0.2010	0.9760
	Prior (3)	$\phi = 0.9$	0.0002	0.1810	0.0033	0.0203	0.0035	0.2013	0.9920
		$= 0.8$	0.0001	0.1810	0.0031	0.0203	0.0032	0.2013	1.0004
		$= 0.7$	0.0001	0.1810	0.0031	0.0203	0.0032	0.2013	1.0010

Table 4: Average squared bias, variance and mean square error related to Case II when a Bayesian approach has been applied. Model II with Algorithm II has been implemented and Priors (2) and (3) have been imposed on the vector of Bernoulli variables γ .

3.2 Detecting Where the Slopes Are Nonzero

Our modeling approach allows for nonstationarity in the B surface, and in particular, it is possible that the relationship between the y and x surfaces vary over space. Therefore, it is of interest to detect the regions where the response has a strong relationship with the covariate. This is equivalent to detecting the locations or pixels on the image where the slopes deviate from zero. To accomplish this, we construct a $100(1 - \alpha)\%$ credible interval for $B(\mathbf{s})$ at each pixel \mathbf{s} . If the credible interval at \mathbf{s} excludes zero, then that gives evidence that $B(\mathbf{s})$ deviates from zero. Note that the upper and lower bounds of all the credible intervals form two-dimensional surfaces which together we call an uncertainty band. Unlike one-dimensional wavelet regression problem where the graphical demonstration of uncertainty bands is feasible (see, e.g., Chipman *et al.* 1997), it is difficult to effectively plot the two-dimensional uncertainty bands. In this section, we use an alternative method to address this difficulty. Before proceeding further, we perform some useful calculations.

We denote $B_i = B(\mathbf{s}_i)$, and let $\mathbf{b}^{(1)}, \dots, \mathbf{b}^{(T)}$ be T posterior samples of \mathbf{b} , where \mathbf{b} denotes the vector of wavelet coefficients of the surface B . Let $B_i^{(t)} = W(\mathbf{s}_i)\mathbf{b}^{(t)}$ for $t = 1, \dots, T$. The Bayesian estimate of B_i is

$$\hat{B}_i = \sum_{t=1}^T B_i^{(t)} / T = W(\mathbf{s}_i)\hat{\mathbf{b}},$$

where $\hat{\mathbf{b}} = \sum_{t=1}^T \mathbf{b}^{(t)} / T$. The posterior variance of $B_i^{(t)}$, $t = 1, \dots, T$, is

$$\hat{\sigma}_i^2 = W(\mathbf{s}_i)\hat{\Sigma}W(\mathbf{s}_i)',$$

where $\hat{\Sigma} = \sum_{t=1}^T (\mathbf{b}^{(t)} - \hat{\mathbf{b}})(\mathbf{b}^{(t)} - \hat{\mathbf{b}})' / (T - 1)$ is an $m \times m$ matrix. We call $\hat{\sigma}_i$ the posterior standard deviation (PSD) of B at pixel \mathbf{s}_i .

We find the pixels at which the slopes deviate from zero, and also classify the pixels according to the magnitudes and signs of the slopes. For this purpose, we construct a choropleth map to indicate $\hat{B}_i \geq \Delta$, $0 \leq \hat{B}_i < \Delta$, $-\Delta < \hat{B}_i < 0$ and $\hat{B}_i \leq -\Delta$, with $\Delta > 0$ a suitably selected threshold.

In the simulated and real data examples discussed later, a majority of the posterior distributions $p(B_i|\mathbf{y}, X)$ of B_i are unimodal and roughly symmetric. Therefore, it is convenient to approximate $p(B_i|\mathbf{y}, X)$ by a normal distribution with center and scale being \hat{B}_i

and $\hat{\sigma}_i$. Using an analogy to the concept of frequentist p -value, if $|\hat{B}_i/\hat{\sigma}_i| > 1.96$, then we believe with strong evidence that $B_i \neq 0$ and represent this situation by $p < 0.05$; if $1.64 \leq |\hat{B}_i/\hat{\sigma}_i| \leq 1.96$, then we believe with moderate evidence that $B_i \neq 0$ and represent this situation by $0.05 \leq p \leq 0.1$; otherwise, we believe that B_i might be close to zero and represent this situation by $p > 0.1$. Note that this is analogous to the interpretation of a frequentist p -value. In a choropleth map, we designate the various possibilities for p by different using different line-patterns.

In a simulation study, the A surface was defined as in Section 3.1 and the B surface was defined by Case II in Section 3.1, i.e., $B(s_1, s_2) = 4 \sin(2\pi s_1) \cos(2\pi s_2)$, $0 \leq s_1, s_2 \leq 1$. Note that B is smooth with zero values at some pixels. Algorithm I under Model I was implemented, and we set $\Delta = 2$ which is half of the maximum value of $|B|$.

In addition, we chose $J = 4$ and generated data from model (2.1) with $\sigma = 1$. Thus, $n = 4096$ and $m = 2048$. We chose the hyperparameters $\mu = \nu = 6$ and prior (3) defined in Section 3.1 was used for the Bernoulli variable γ for each of the cases $\phi = 1, 0.9, 0.8, 0.7$. Markov chains of length 5000 were simulated with the first half burn-ins, and we used the second half for calculations. Convergence was assessed through Gelman-Rubin's factors.

Figure 2 displays the images of \hat{B} and the PSD of B corresponding to $\phi = 1, 0.9, 0.8, 0.7$ when using x_c defined in Section 4.1 as the covariate surface. We observe that all the \hat{B} images graphically resemble the true B , and the PSD of B for $\phi = 1$ appear to be greater than those for $\phi = 0.9, 0.8, 0.7$. We also observe that when ϕ decreases, the \hat{B} images become slightly sparser in the sense that larger square regions appear on the images. This is because when the Bernoulli probabilities associated with higher level wavelet coefficients become smaller, the finer details will be dropped and the basis supports with smaller sizes will merge into larger square regions.

As displayed in Figure 2, there are three peaks (indicated by red) and three valleys (indicated by blue) regularly arranged on the true B image, and the values of the true B at the pixels around the peaks and valleys deviate from zero, while they are close to zero elsewhere. Figure 3 displays the choropleth map for \hat{B} corresponding to various ϕ values. We observe that the locations where the B values deviate from zero are correctly detected and changing ϕ makes little change in the detection results.

3.3 Applications to Gypsy Moth Defoliation Data

We next use the proposed Bayesian approach to analyze the gypsy moth defoliation data introduced in Section 1. Recall that the defoliation data contains images of defoliation rates (response) and elevations (covariate). The images consist of 64×64 evenly spaced pixels \mathbf{s}_i s, and therefore, $n = 4096$. The response $y(\mathbf{s})$ and the covariate $x_1(\mathbf{s})$ represent the centered-and-scaled defoliation rate and scaled elevation measured at pixel \mathbf{s} respectively (as displayed in Figure 1). We used the centered-and-scaled x_1 as the covariate surface x , i.e., $x(\mathbf{s}) = (x_1(\mathbf{s}) - \overline{vec(x_1)})/\text{std}(vec(x_1))$, where $vec(x_1)$ denotes the vector of x_1 values at the 4096 pixels, and $\overline{vec(x_1)}$ and $\text{std}(vec(x_1))$ are the sample mean and standard deviation of $vec(x_1)$. $J = 4$ was used, and thus, $m = 2048$ wavelet coefficients are involved in our model.

We fixed $\mu = \nu = 6$ and fit Model I. Prior (1) was placed on γ with the Bernoulli probabilities corresponding to resolution levels 0 to 4 being $0.5, 0.5\phi, 0.5\phi^2, 0.5\phi^3$ and $0.5\phi^4$ respectively. We somewhat arbitrarily chose $\phi = 0.9$ to produce some degree of flatness in the estimates. A Markov chain of length 20,000 was simulated from the posterior distribution $p(\beta, \gamma, \sigma, \tau | \mathbf{y}, X)$ specified by (2.2) using Algorithm I, and the first half was treated as burn-ins. The initial point $\beta^{(0)}$ for the β chain was generated from $N(\hat{\beta}, 10^{-4}I_m)$, where $\hat{\beta}$ was chosen as the least squares estimate of β . It took about 2.25 hours to draw 10,000 posterior samples. Convergence was assessed by applying Gelman-Rubin factors to 5 parallel Markov chains. We also applied the method introduced in Section 3.2 to classify the pixels.

Figure 4 displays the estimated intercept \hat{A} , the estimated slope \hat{B} , the fitted defoliation rate \hat{y} and the PSD of the slope B . In particular, the images of \hat{A} , \hat{B} and the PSD were constructed over a 100×100 lattice set of locations in $[0, 1) \times [0, 1)$ to display the posterior samples at new locations; while the \hat{y} image was constructed over the 64×64 lattice set of locations in $[0, 1) \times [0, 1)$ where the data were drawn allowing us to compare \hat{y} with y at the observed locations. We observe that \hat{B} is positive at most of the pixels, which shows an overall positive relationship between the defoliation rate and elevation. Furthermore, \hat{B} is slightly smaller at the locations where the elevation is small. We also observe that in the regions where the elevation changes quickly, the PSD of the slope deviates considerably from zero. Finally, the image \hat{y} appears to resemble the observed defoliation rate image y . Our findings on \hat{B} and \hat{y} are similar to those made by Zhang *et al.* (2011) who used LASSO algorithm to perform the computations, but again, we are also able to characterize the uncertainty in the relationships.

Figure 5 displays the choropleth map of the slope in which we chose $\Delta = 0.8$ (about 1/3 the maximum of $|\hat{B}|$). We observe that in the upper-left region, the relationship between defoliation rate and elevation is strong and positive, while in the nearly central region, the relationship between defoliation rate and elevation is not strong. We also observe that, at a small number of locations, $p < 0.05$ and $B \leq -0.8$ which shows that the relationship there is strong and negative.

4 Discussion

Zhang *et al.* (2011) applied a wavelet approach to transform the spatial concurrent linear model into a linear model with design matrix induced by a wavelet structure, and they implemented LASSO to handle the estimation problem. With their approach, however, it is difficult to conduct inferences using their method. To address this, we have developed a Bayesian variable selection approach based on the model proposed by Zhang *et al.* (2011). Specifically, we applied a Bayesian model similar to one proposed by George and McCulloch (1993), in which we introduced a vector γ of Bernoulli variables for the model coefficients so that the selection and estimation of the nonzero coefficients can be simultaneously achieved. The proposed approach is highly flexible and computationally efficient, and should be useful in many practical situations where the data display complex nonstationary patterns. In addition, we developed a Gibbs sampler for posterior sampling that involves no complicated matrix computation. Hence, this is efficient for handling relatively large datasets. Furthermore, as demonstrated in simulated and real data analysis, our approach is effective in detecting the spatial locations where the response has a relationship with a covariate, and provides statistical evidence for such detections.

We have placed Bernoulli priors on γ . Other priors such as Markov chain priors can also be applied by invoking a tree structure (see Romberg *et al.*, 2001). The support of any Haar wavelet basis function, which we call a parent, is divided into four equal adjacent pieces at the same level, which we call children, with each piece being the support of a Haar wavelet basis function. Since any basis support corresponds to a 0-1 variable γ_j , we also call $\gamma_{j'}$ the parent of γ_j if their corresponding basis supports have such parent-children relationship. Following Romberg *et al.* (2001), a Markov chain prior is defined to be

$$p(\gamma_j | \gamma_{-j}) = p(\gamma_j | \gamma_{j'}), \quad (4.1)$$

where $\gamma_{-j} = \{\gamma_i | i \neq j\}$, and $\gamma_{j'}$ is the parent of γ_j . The equation (4.1) means that the distributional properties of a child only depends on its parent. Let the transition probability be $p(\gamma_j | \gamma_{j'}) = p_{\gamma_{j'}, \gamma_j}$. We have numerically examined Markov chain priors with $p_{0,0} = 0.9$, $p_{0,1} = 0.1$, $p_{1,0} = 0.1$, $p_{1,1} = 0.9$, and found that they did not perform as well as Bernoulli priors and LASSO when estimating a piecewise constant surface. The reason might be that a piecewise constant surface has too much local flatness, and hence, even if a parent corresponds to a nonzero wavelet coefficient, its four children may still correspond to zero wavelet coefficients, which makes the connection between the parent and children weak. Under such circumstances, Bernoulli priors which assume independence among the basis functions may be better choices.

Two future extensions of the current work might be also worth mentioning. First, Dunson (2009) proposed a nonparametric Bayesian approach to model the basis coefficients in a longitudinal model. In his method, the prior distribution of the basis coefficients is nonparametric; in particular, they used a Dirichlet process prior, which provides a great deal of flexibility. Dunson (2009) found that the nonparametric prior works well for modeling the model coefficients, and it seems reasonable to extend that work to our model.

Second, in our model, the coefficients are sparse, and so even if the the number of parameters is large, the estimation results are still satisfactory. Although a sparse coefficient vector is common in the regression models associated with wavelets, it is still interesting to fit a model with non-sparse coefficients and examine the results. One article about the identification of the sparseness pattern of the model coefficients is given by Meinshausen and Yu (2009) who examined the impact of sparseness on LASSO estimates. There seems to be little literature handling this problem under a Bayesian framework, and so we intend to explore this further in the future.

Supplement Material: Sampler derivations for algorithm I can be found in the first author's website <http://www.stat.wisc.edu/~shang/>

Acknowledgments The authors would like to thank the Editor, an associate editor and the anonymous referees for valuable and constructive suggestions leading to substantial improvements in the article. The authors also thank Bret Larget, Kam Tsui, Jun Zhu, Rick Nordheim and Jun Shao for many useful suggestions on this paper.

References

- [1] Brown, P., Fearn, T. and Vannucci, M. (2001). Bayesian Wavelet Regression on Curves With Application to a Spectroscopic Calibration Problem. *Journal of the American Statistical Association*, **96**, 398–408.
- [2] Brown, P., Vannucci, M. and Fearn, T. (2002). Bayes Model Averaging with Selection of Regressors. *Journal of the Royal Statistical Society, Series B*, **64**, 519–536.
- [3] Casella, G., Girón, F. J., Martínez, M. L. and Moreno, E. (2009). Consistency of Bayesian Procedures for Variable Selection. *The Annals of Statistics*, **37**, 1207–1228.
- [4] Chipman, H., Kolaczyk, E. and McCulloch, R. (1997). Adaptive Bayesian Wavelet Shrinkage. *Journal of the American Statistical Association*, **92**, 1413–1421.
- [5] Clyde, M. and George, E. (2000). Flexible Empirical Bayes Estimation for Wavelets. *Journal of the Royal Statistical Society, Series B*, **62**, 681–698.
- [6] Clyde, M., Parmigiani, G. and Vidakovic, B. (1998). Multiple Shrinkage and Subset Selection in Wavelets. *Biometrika*, **85**, 391–401.
- [7] Crouse, M. S., Nowak, R. D. and Baraniuk, R. G. (1998). Wavelet-Based Statistical Signal Processing Using Hidden Markov Models. *IEEE Transactions on Signal Processing*, **46**, 886–902.
- [8] Daubechies, I. (1992). *Ten Lectures on Wavelets*. CBMS-NSF Regional Conference Series in Applied Mathematics 61.
- [9] Dunson, D. (2009). Nonparametric Bayes Local Partition Models for Random Effects. *Biometrika*, **96** 249–262.
- [10] Fan J., Wu, Y. and Feng, Y. (2010). Local Quasi-likelihood With a Parametric Guide. *The Annals of Statistics*, **37**, 4153–4183.
- [11] Fernández, C., Ley, E., and Steel, M. F. (2001). Benchmark Priors for Bayesian Model Averaging. *Journal of Econometrics*, **100**, 381–427.
- [12] Gelman, A., Carlin, J. B., Stern, H. S. and Rubin, D. B. (2003). *Bayesian Data Analysis* (2nd ed). Chapman & Hall/CRC.
- [13] George, E. and McCulloch, R. (1993). Variable Selection via Gibbs Sampling. *Journal of the American Statistical Association*, **88**, 881–889.
- [14] Godsill, J. S. and Rayner, P. J. W. (1998). Robust Reconstruction and Analysis of Autoregressive Signals in Impulsive Noise Using the Gibbs Sampler. *IEEE Transactions on Speech and Audio Processing*, **6**, 352–372.

- [15] Jiang, W. (2007). Bayesian Variable Selection for High Dimensional Generalized Linear Models: Convergence Rates of the Fitted Densities. *The Annals of Statistics*, **35**, 1487–1511.
- [16] Jiang, W. and Tanner, M. (2008). Gibbs Posterior for Variable Selection in High-Dimensional Classification and Data Mining. *The Annals of Statistics*, **36**, 2207–2231.
- [17] Kleiner, K. and Montgomery, M. (1994). Forest Stand Susceptibility to the Gypsy–Moth (lepidoptera, lymantriidae)–Species and Site Effects on Foliage Quality to Larvae. *Environmental Entomology*, **23**, 699–711.
- [18] Liang, F., Paulo, R., Molina, G., Clyde, M. and Berger, J. (2008). Mixtures of g -Priors for Bayesian Variable Selection. *Journal of the American Statistical Association*, **103**, 410–423.
- [19] Li, F. and Zhang, N. R. (2010). Bayesian Variable Selection in Structured High-Dimensional Covariate Spaces with Applications in Genomics. *Journal of the American Statistical Association*, **105**, 1202–1214.
- [20] Meinshausen, N. and Yu, B. (2009). LASSO-type Recovery of Sparse Representations for High-Dimensional Data. *The Annals of Statistics*, **37**, 246–270.
- [21] Moreno, E., Girón, F. J. and Casella, G. (2010). Consistency of Objective Bayes Factors as the Model Dimension Grows. *The Annals of Statistics*, **38**, 1937–1952.
- [22] Nott, D. and Green, P. (2004). Bayesian Variable Selection and Swendsen-Wang Algorithm. *Journal of Computational and Graphical Statistics*, **13**, 141–157.
- [23] Romberg, J., Choi, H. and Baraniul, R. (2001). Bayesian Tree-Structured Image Modeling Using Wavelet-Domain Hidden Markov Models. *IEEE Transactions on Image Processing*, **10**, 1056–1068.
- [24] Shang, Z. and Clayton, M. K. (2010). Consistency of Bayesian Model Selection for Linear Models With A Growing Number of Parameters. *Journal of Statistical Planning and Inference*, in press.
- [25] Smith, M. and Fahrmeir, L. (2007). Spatial Bayesian Variable Selection With Application to Functional Magnetic Resonance Imaging. *Journal of the American Statistical Association*, **102**, 417–431.
- [26] Townsend, P. A., Eshleman, K. N. and Welcker, C. (2004). Remote Sensing of Gypsy Moth Defoliation to Assess Variations in Stream Nitrogen Concentrations. *Ecological Applications*, **14**, 504–516.

- [27] Wheeler, D. C. (2009). Simultaneous coefficient penalization and model selection in geographically weighted regression: the geographically weighted lasso. *Environment and Planning A* **41**, 722–742.
- [28] Wheeler D. C., and Waller L. A. (2009). Comparing spatially varying coefficient models: a case study examining violent crime rates and their relationships to alcohol outlets and illegal drug arrests. *Journal of Geographical Systems* **11**, 1–22.
- [29] Wolfe, P., Godsill, S. and Ng, W. (2004). Bayesian Variable Selection and Regularization for Time-Frequency Surface Estimation. *Journal of the Royal Statistical Society, Series B*, **66**, 575–589.
- [30] Yuan, M. and Lin, Y. (2005). Efficient Empirical Bayes Variable Selection and Estimation in Linear Models. *Journal of the American Statistical Association*, **100**, 1215–1225.
- [31] Zhang, J., Clayton, M. K. and Townsend, P. A. (2011). Functional Concurrent Linear Regression Model for Spatial Images. *Journal of Agricultural, Biological and Environmental Statistics*, **16**, 105–130.

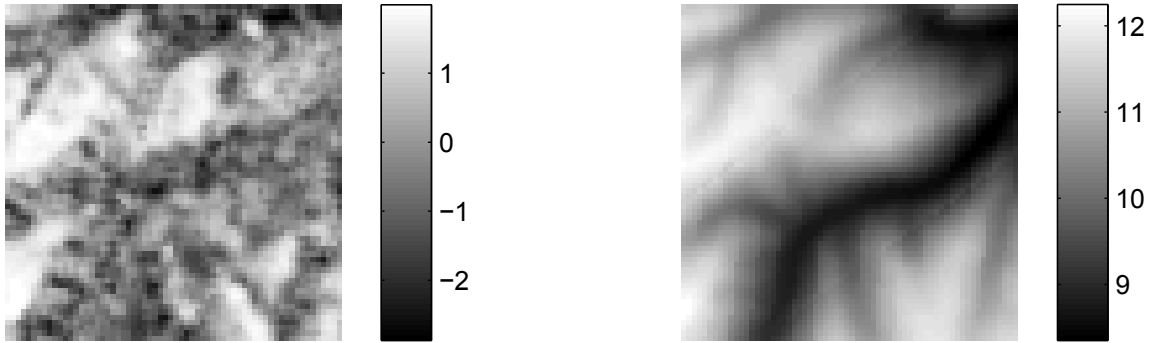


Figure 1: *Images of gypsy moth defoliation data. The left panel is the image of centered-and-scaled defoliation rate and the right panel is the image of scaled elevation. Low to high data values are represented by black to white tones. The defoliation rate and elevation respectively represent the proportion of defoliated forest and height on a per-pixel basis, and both of the images have 30m pixel resolution. The defoliation rate data were obtained through Landsat satellite imaging and the elevation data were obtained by the National Elevation Data set of the US Geological Survey.*

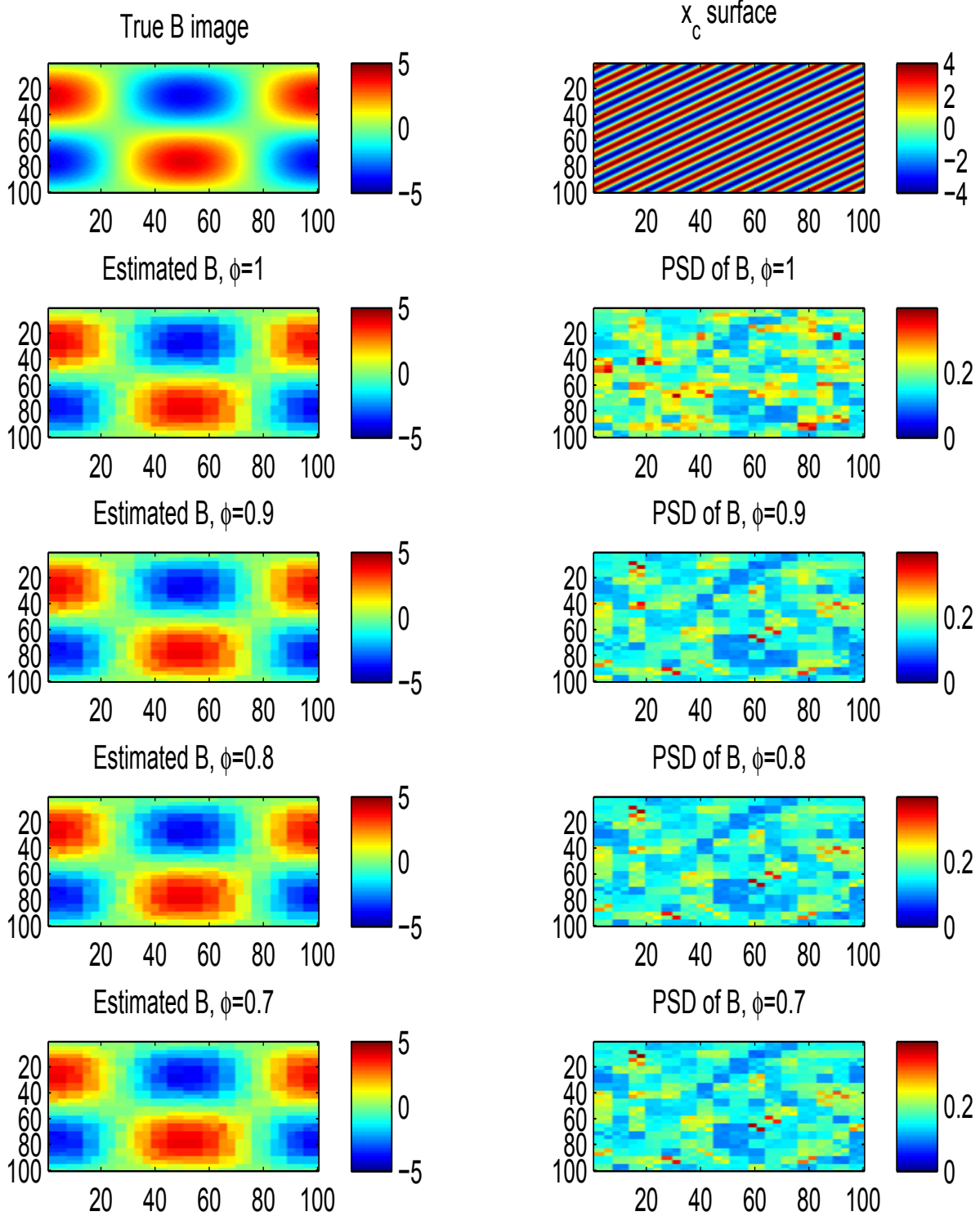


Figure 2: Section 3.2. Images of estimated B and the PSD of B for $\phi = 1, 0.9, 0.8, 0.7$. Covariate surface x_c and Prior (3) were used. Images of the true B and x_c are also shown.

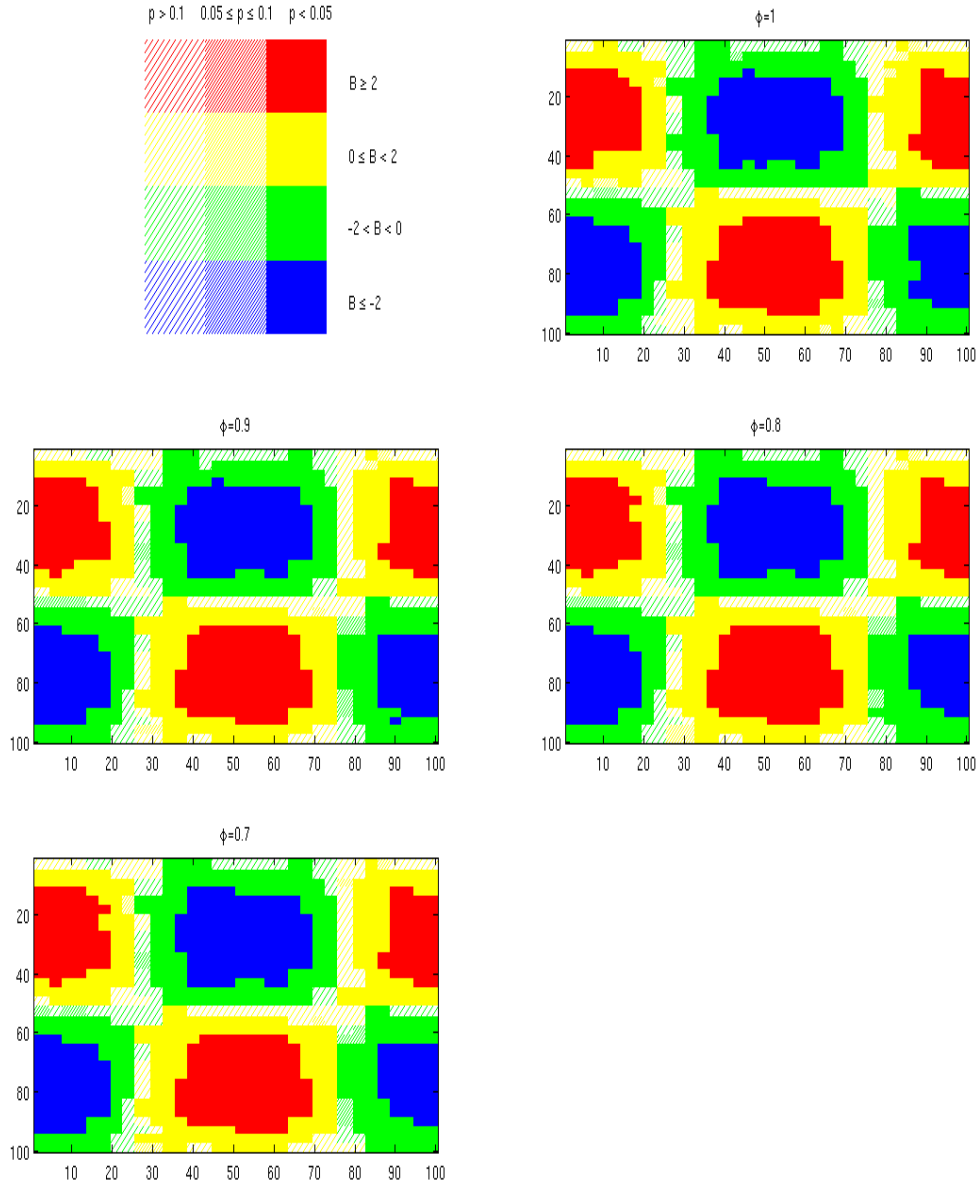


Figure 3: Section 3.2. Choropleth map of \hat{B} for $\phi = 1, 0.9, 0.8, 0.7$. Covariate surface x_c and Prior (3) were used. Red indicates $\hat{B}_i \geq 2$; Yellow: $0 \leq \hat{B}_i < 2$; Green: $-2 < \hat{B}_i < 0$; Blue: $\hat{B}_i \leq -2$. Filled boxes: $p < 0.05$; boxes with dense lines: $0.05 \leq p \leq 0.1$; boxes with thin lines: $p > 0.1$.

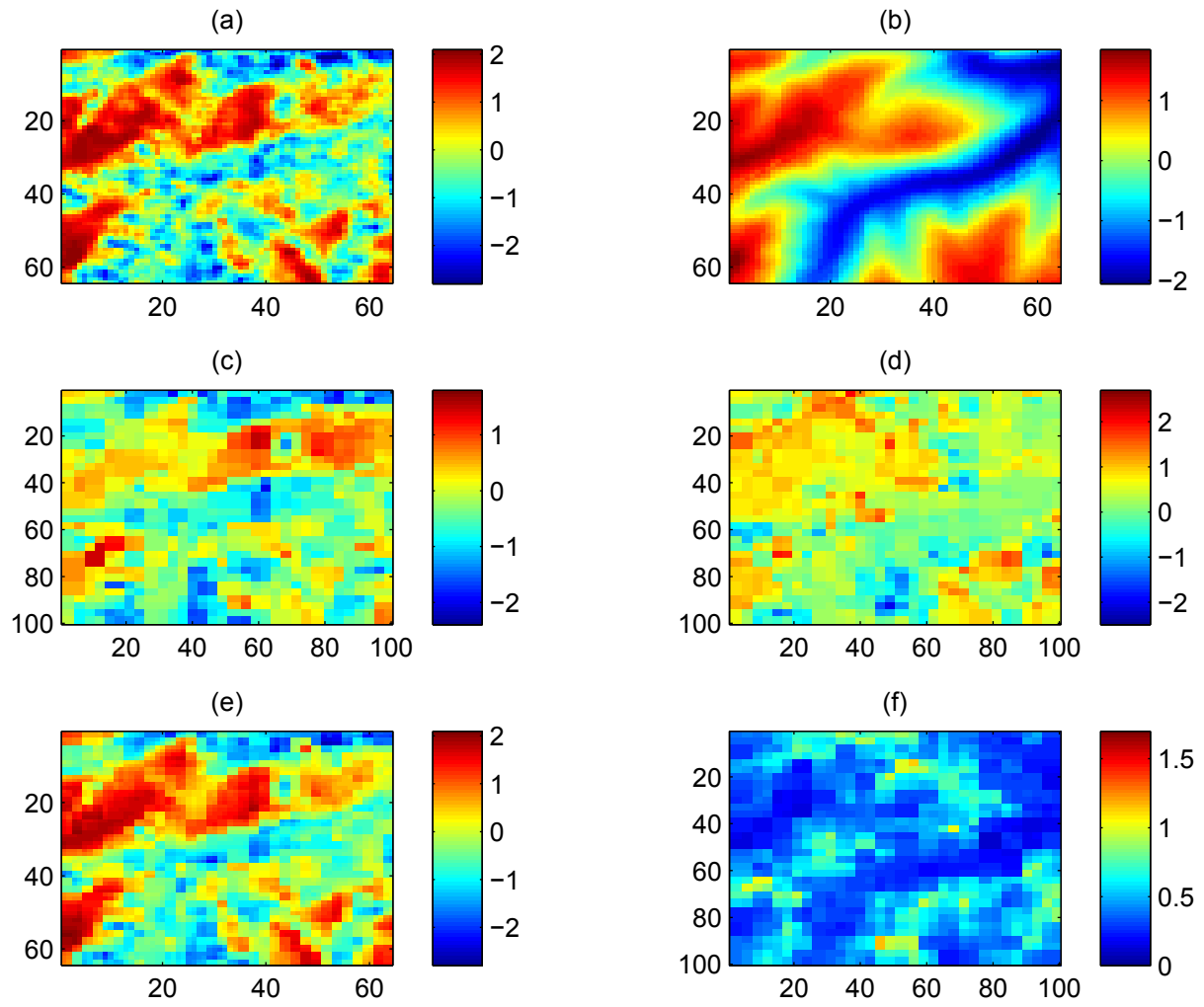


Figure 4: (a): Centered-and-scaled defoliation rate y ; (b): Centered-and-scaled elevation x ; (c): Estimated intercept \hat{A} ; (d): Estimated slope \hat{B} ; (e): Fitted value \hat{y} ; (f): PSD of the slope B . Prior (1) with $\phi = 0.9$ was used.

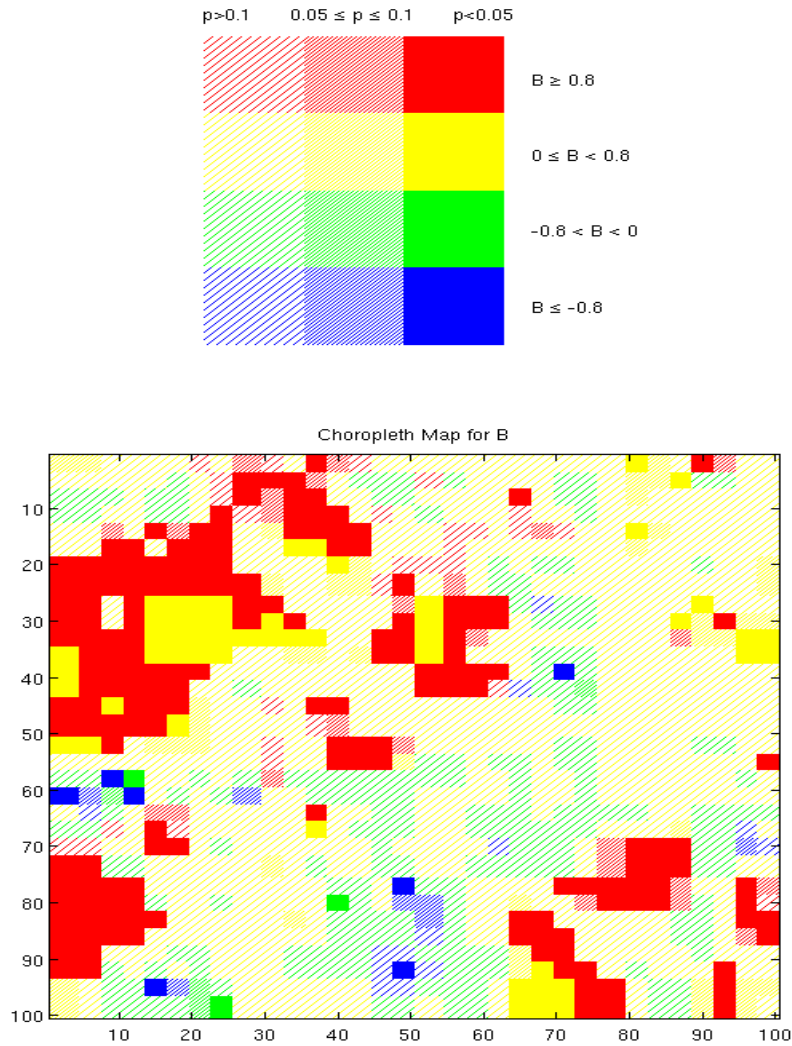


Figure 5: Choropleth map for the slope surface B . Prior (1) with $\phi = 0.9$ was used. Red indicates $\hat{B}_i \geq 0.8$; Yellow: $0 \leq \hat{B}_i < 0.8$; Green: $-0.8 < \hat{B}_i < 0$; Blue: $\hat{B}_i \leq -0.8$. Filled boxes: $p < 0.05$; boxes with dense lines: $0.05 \leq p \leq 0.1$; boxes with thin lines: $p > 0.1$.